Axisymmetric balance dynamics of tropical cyclone intensification: Diabatic heating versus surface friction

Roger K. Smith[a]*and Shanghong Wang[a]
[a] *Meteorological Institute, Ludwig-Maximilians University of Munich, Munich, Germany*
*Correspondence to: Prof. Roger K. Smith, Meteorological Institute, Ludwig-Maximilians University of Munich, Theresienstr. 37, 80333 Munich. E-mail: roger.smith@lmu.de

The evolution of an idealized tropical-cyclone-like vortex forced by a prescribed distribution of diabatic heating rate and near surface frictional force is studied using a recently-developed prognostic axisymmetric balance model. Starting with a prescribed initial tangential wind field, a series of calculations is carried out in which the strength of the diabatic heating rate is varied while keeping the strength of the frictional force fixed. When the strength of the heating rate falls below a certain value, the secondary circulation it generates is no longer able to oppose the tendency of the boundary layer to produce a layer of low-level outflow in the lower troposphere, above the boundary layer. In these circumstances, the net outflow just above the boundary layer advects absolute momentum surfaces outwards and the tangential velocity there declines. In the balance model, and presumably in reality, intensification of the tangential velocity requires the diabatic heating rate to be strong enough to ventilate the inflow in the frictional boundary layer, thereby averting frictionally-induced outflow just above the boundary layer. In reality, the strength and location of diabatic heating will be strongly influenced by the boundary layer dynamics and thermodynamics, a coupling not present in the current balance model formulation.

Key Words: Hurricane; tropical cyclone; typhoon; boundary layer; vortex intensification

Received April 6, 2018; Revised ; Accepted

Citation: . . .

1. Introduction

In a recent paper, Smith et al. (2018) [henceforth SMB] presented simulations of tropical cyclone intensification in the framework of an idealized axisymmetric prognostic balance formulation. The main focus of their study was to examine the amplification of the tangential wind field, the kinematic structure and evolution of the primary and secondary circulation in physical space, and the ultimate development of localized regions where the flow becomes symmetrically and/or statically unstable. In such regions, the SE-equation is no longer elliptic and to obtain balance solutions under these circumstances, the SE-equation must be regularized in the unstable regions to keep it elliptic globally. Even so, regularization does not suppress the development of instabilities and the extended solutions ultimately break down. Thus, there is a limit to the time over which the balance model can be integrated.

The foregoing study was motivated in part by a desire to determine the flow structure near the base of the eyewall in a balance framework. In the classical axisymmetric paradigm for vortex spin up (Ooyama 1969), diabatic heating brought about by the collective effects of deep convection in some inner region of a modest strength vortex are invoked to produce inflow in the lower troposphere. Above the frictional boundary layer, absolute angular momentum, M, is approximately materially conserved, and since the radial

gradient of M is typically positive, the inflow draws the M-surfaces inwards leading to spin up[1].

Friction in a surface-based boundary layer leads to inflow in that layer, but because the frictional torque there reduces M, the inflow does not necessarily lead to a local amplification of v. In the absence of deep convection, the frictionally-induced inflow would lead through continuity[2] to a layer of outflow above the boundary layer (Willoughby 1979) and thereby to a spin down of the tangential wind in this layer as M-surfaces are advected outwards.

Because of space limitations, SMB, presented only one simulation in which the combined effects of surface friction[3] and diabatic heating were present. However, the ensuing flow is expected to depend on the relative importance of both processes, since, as noted above, while both lead to inflow near the surface, friction would, by itself, lead to outflow above the frictional boundary layer. Thus, vortex intensification by the classical mechanism requires that the diabatically forced inflow above the boundary layer is strong enough to offset the frictionally induced outflow there.

It is reasonable to surmise that, in reality, the ability of deep convection to ventilate the mass of air converging in the boundary layer depends, *inter alia*, on the degree of convective instability and hence on the moisture of the ascending air. However, the rate at which air converges in the boundary layer depends to a significant degree, through boundary layer dynamics, on the radial structure of the gradient wind at the top of the boundary layer. Again, it is the relative importance of these two separate processes that determine whether spin up will occur (see e.g. Kilroy et al. 2016). The relative importance of these two processes will influence the pattern of streamflow in the lower troposphere in relation to the M-surfaces, which, above the boundary layer determines whether the flow will locally spin up or spin down. At this point, it may be worth remarking that a common assumption in past theoretical studies is that *all* of the air that converges in the boundary layer ascends in deep convection to the upper troposphere (e.g. Ooyama 1969; Emanuel 1997, 2012).

The purpose of the present paper is to explore the dependence of vortex intensification on the heating rate and friction by carrying out simulations of the prognostic balance model of SMB in which the strength of diabatic forcing is varied while keeping the surface drag coefficient fixed. As in SMB, the primary aim is to provide a context for a more complete understanding of how departures from the classical model for tropical cyclone spin up come about in numerical models and in observations.

1.1. *The prognostic balance model*

Full details of the prognostic balance model are given in SMB. In brief, the model is formulated in cylindrical r-z coordinates. The prognostic element is the tendency equation for tangential wind component v, which has the form:

$$\frac{\partial v}{\partial t} = -u\frac{\partial v}{\partial r} - w\frac{\partial v}{\partial z} - \frac{uv}{r} - fu - \dot{V}, \qquad (1)$$

where u and w are the radial and vertical velocity components, t is the time, f is the Coriolis parameter (assumed constant), and $\dot{V}$ is the azimuthal momentum sink associated with the near-surface frictional stress. The balanced density field is obtained from the thermal wind equation, which has the general form:

$$\frac{\partial}{\partial r}\log\chi + \frac{C}{g}\frac{\partial}{\partial z}\log\chi = -\frac{\xi}{g}\frac{\partial v}{\partial z}, \qquad (2)$$

where $\chi = 1/\theta$ is the inverse of potential temperature θ, $C = v^2/r + fv$ is the sum of centrifugal and Coriolis forces per unit mass, $\xi = f + 2v/r$ is the modified Coriolis (inertia) parameter, i.e. twice the local absolute angular velocity, and g is the acceleration due to gravity. This is a first order partial differential equation for $\log\chi$, which on an isobaric surface is equal to the logarithm of density ρ plus a constant, with characteristics $z_c(r)$ satisfying the ordinary differential equation $dz_c/dr = C/g$.

The streamfunction ψ for the secondary circulation is obtained by solving the Sawyer-Eliassen (SE) equation:

$$\frac{\partial}{\partial r}\left[-g\frac{\partial\chi}{\partial z}\frac{1}{\rho r}\frac{\partial\psi}{\partial r} - \frac{\partial}{\partial z}(\chi C)\frac{1}{\rho r}\frac{\partial\psi}{\partial z}\right] +$$
$$\frac{\partial}{\partial z}\left[\left(\chi\xi\zeta_a + C\frac{\partial\chi}{\partial r}\right)\frac{1}{\rho r}\frac{\partial\psi}{\partial z} - \frac{\partial}{\partial z}(\chi C)\frac{1}{\rho r}\frac{\partial\psi}{\partial r}\right] =$$
$$g\frac{\partial}{\partial r}\left(\chi^2\dot{\theta}\right) + \frac{\partial}{\partial z}\left(C\chi^2\dot{\theta}\right) + \frac{\partial}{\partial z}\left(\chi\xi\dot{V}\right) \qquad (3)$$

where $\zeta = (1/r)\partial(rv)/\partial r$ is the vertical component of relative vorticity, $\zeta_a = \zeta + f$ is the absolute vorticity and $\dot{\theta} = d\theta/dt$ is diabatic heating rate. The derivation of this equation is sketched in section 2.2 of Bui et al. (2009). The transverse velocity components u and w are given in terms of ψ by:

$$u = -\frac{1}{r\rho}\frac{\partial\psi}{\partial z}, \qquad w = \frac{1}{r\rho}\frac{\partial\psi}{\partial r}. \qquad (4)$$

The discriminant of the SE-equation, Δ, is given by

$$\Delta = \gamma^2\left[-\frac{g}{\chi}\frac{\partial\chi}{\partial z}\left(\xi\zeta_a + \frac{C}{\chi}\frac{\partial\chi}{\partial r}\right) - \left(\frac{1}{\chi}\frac{\partial}{\partial z}(C\chi)\right)^2\right], \qquad (5)$$

where $\gamma = \chi/(\rho r)$, and the SE-equation is elliptic if $\Delta > 0$.

The prescribed diabatic heating rate has the same spatial form as in SMB. The heating rate distribution varies sinusoidally with height with a maximum amplitude at an altitude of 8 km and is zero above the tropopause (16 km). In the radial direction, the distribution has a skewed bell-shape in radius (inner radius 20 km, outer radius 70 km scale) and the maximum amplitude is centred on a particular M surface at a height of 1 km. This M surface was chosen to have the value 8.7×10^5 m^2 s^{-1}, corresponding with a potential radius $\sqrt{2M/f}$ of 265 km, which lies initially inside the radius of maximum tangential wind speed. In the control experiments, the maximum amplitude is 3 K h^{-1}.

[1] $M = rv + \frac{1}{2}fr^2$, where r is the radius, v is the tangential velocity and f is the Coriolis parameter. Thus a local increase in M corresponds with a local increase in v.

[2] Strictly one should not argue that continuity causes the upflow, rather continuity, together with boundary conditions on the flow, constrains the pressure field and it is the associated vertical gradient of pressure that drives the upflow.

[3] Of course, in the balance formulation, the effects of friction could be examined only in the limited context of an axisymmetric balanced boundary layer formulation.

In other experiments it is some multiple of this value as detailed in Table I.

The effects of surface friction are represented by a body force corresponding with the surface frictional stress distributed through a boundary layer with uniform depth H. The body force has the same spatial form and same magnitude as that in SMB.

The vertical temperature and moisture structure at large radii is a linear approximation to the Dunion moist tropical sounding (Dunion 2011) as shown in Fig. 1 of SMB. The initial vortex is the same as that in SMB: it has a maximum tangential wind speed of 10 m s^{-1} at a radius of 100 km (the structure may be seen in Figure 2 below).

The method of solution is the same as described in sections 2.2 and 2.3 of SMB. Moreover, as in SMB, the calculations are carried out in a rectangular domain 1000 km in the radial direction and 18 km in the vertical. The grid spacing is uniform in both directions: 5 km in the radial direction and 200 m in the vertical and the integration ime step is one minute. The boundary condition on the SE-equation are that $\psi = 0$ at $r = 0$, $z = 0$ and $z = H$, implying no flow through these boundaries, while the outer radial boundary, $r = r_R$, is taken to be open, i.e. $\partial\psi/\partial r = 0$, implying that $w = 0$ at this boundary.

At early times in all the simulations to be described, the discriminant of the SE-equation, Δ, is positive and the SE-equation is elliptic globally. Nevertheless, as in the cases described SMB, isolated flow regions ultimately develop in which Δ becomes negative and these regions become more extensive in area with time. In these regions, the SE-equation is hyperbolic and the flow satisfies the conditions for symmetric instability. To continue the solution beyond the time at which Δ first becomes negative, a regularization method is required. The regularization scheme used here and its limitations is described in SMB.

2. Results of six simulations

The results of six simulation experiments are presented here. The experiments differ only in the maximum magnitude of the heating distribution as summarized in Table I. The first simulation, Ex-1, is the same as Ex-UF in SMB and serves as a control calculation. As in SMB, each simulation starts with an initial warm-cored vortex that has a maximum tangential wind speed of 10 m s^{-1} at the surface at a radius of 100 km at a latitude of 20^{o}N.

Table I. Summary of the six simulations carried out

Simulation	Maximum heating amplitude
Ex-1	3 K h^{-1} (Control calculation)
Ex-2	3.75 K h^{-1} (1.25 × Control)
Ex-3	4.5 K h^{-1} (1.5 × Control)
Ex-4	1.5 K h^{-1} (0.5 × Control)
Ex-5	0.75 K h^{-1} (0.25 × Control)
Ex-6	0.375 K h^{-1} (0.125 × Control)

2.1. *Flow evolution*

Figure 1(a) shows the evolution of the maximum tangential velocity component in the six simulations and the times at which the SE-equation requires regularization, which depends on the strength of the heating. As expected, the rate of intensification and its sign depend also on the strength of the heating. In experiments Ex-1, Ex-2, Ex-3 and Ex-4, the rate of intensification is positive and increases with the strength of the heating. In experiments Ex-5 and Ex-6, the vortex decays. The time at which the SE-equation requires regularization decreases as the strength of the heating increases as does the time eventual breakdown of the solution. For example, the solution in Ex-3, which has the strongest heating rate, breaks down after only 18 h and the SE equation requires regularization shortly after 6 h. On the other hand, the simulations with the three[4] weakest heating rates ran for more than 15 h before the SE-equation required regularization and the solutions ran for at least 24 h.

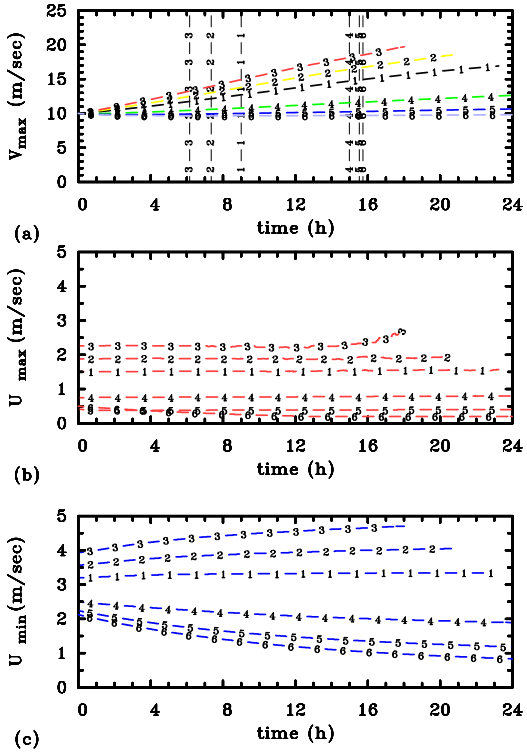

Figure 1. Time series of (a) V_{max}, (b) U_{max} and (c) U_{min} for the simulations Ex-1 to Ex-6. The dashed vertical lines indicate the time at which the regularization is first required for each simulation.

Figures 1(b) and (c) show the evolution of the maximum (U_{max}) and minimum (U_{min}) radial velocity component in the six simulations. As expected U_{max} increases as the magnitude of the diabatic heating increases, except at early times when it is slightly larger in Ex-6 than in Ex-5. In most simulations, U_{max} remains more or less uniform with time, the exceptions being Ex-3, where U_{max} begins to increase after about 16 h and in Ex-6 where it slowly decreases. At any given time, the magnitude of U_{min} increases as the magnitude of the diabatic heating increases, but in the Ex-1, Ex-2 and Ex-3 simulations, the magnitude increases also with time, while in the Ex-4, Ex-5 and Ex-6 simulations, it decreases in magnitude with time reflecting the increasing dominance of friction compared with heating.

[4]Interestingly, the solution in the control experiment breaks down shortly before 24 h, while in the identical simulation reported in SMB, the calculation ran for a little more than 24 h. Further exploration of this issue suggests that the ultimate time breakdown is somewhat machine dependent and it depends a little also on the time step used, which is the same in the present calculations and those of SMB.

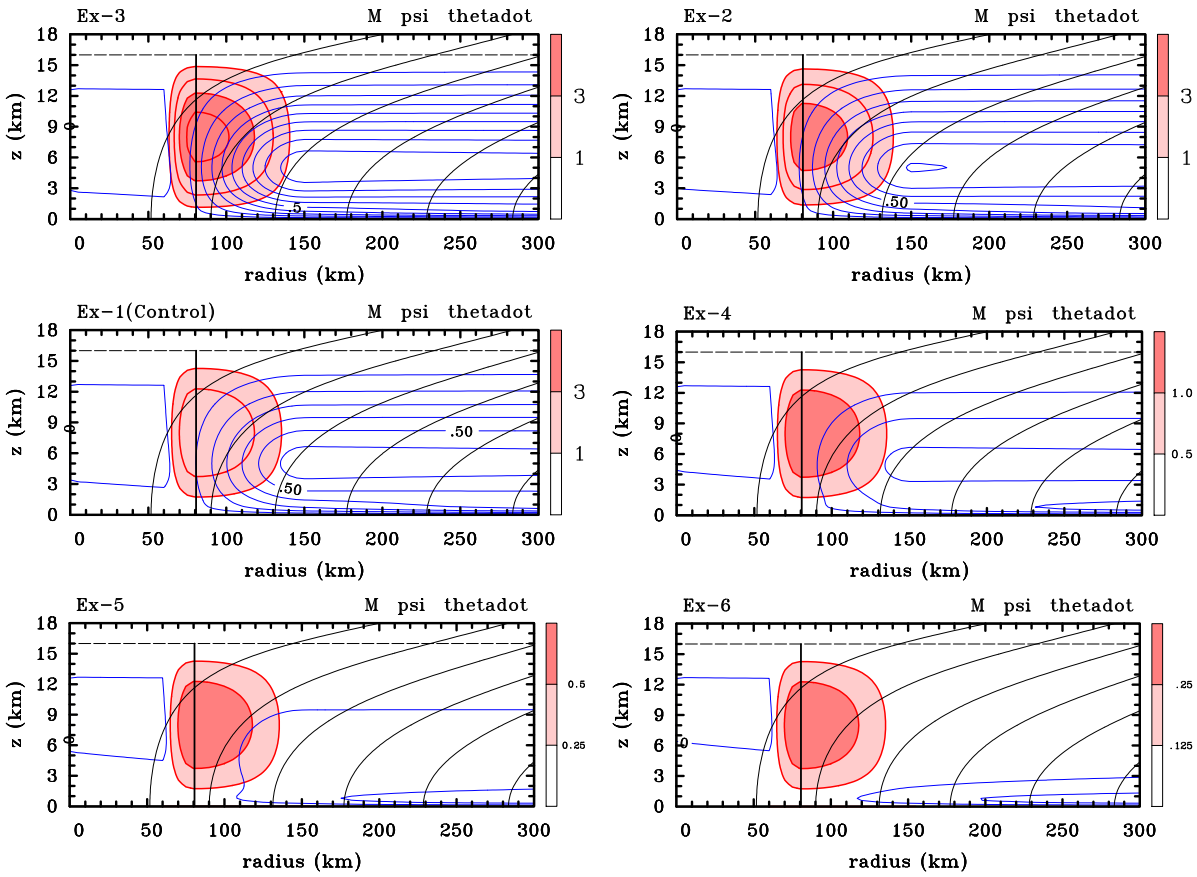

Figure 2. Radius-height cross sections of M-surfaces superimposed on the streamlines of the secondary circulation, ψ, and diabatic heating rate $\dot{\theta}$ (shaded) at the initial time. The panels are ordered with the strongest heating rate in panel (a), the next strongest in panel (b) and so on. The dashed horizontal line at a height of 16 km indicates the tropopause. The thick vertical line shows the location of the maximum diabatic heating rate. Contour intervals are: for M, 5×10^5 m^2 s^{-1}; for ψ, 1×10^8 kg s^{-1}; for $\dot{\theta}$, in panels (a)-(c) 1 K h^{-1}, in panel (d) 0.5 K h^{-1}, in panel (e) 0.25 K h^{-1}, in panel (f) 0.125 K h^{-1}.

2.2. *Flow structure at the initial time*

Reasons for some of the foregoing behaviour are highlighted by Figure 2, which shows radial-height cross sections of M-surfaces superimposed on the streamlines of the secondary circulation, ψ, and diabatic heating rate $\dot{\theta}$ at the initial time. In experiments Ex-1, Ex-2 and Ex-3, there is an inward upward component of flow across the M-surfaces in the region of heating in the lower troposphere, except near the surface. Thus, the tangential wind in this region willl increase with time as the flow evolves. Moreover, the M-surface to which the heating is ti ed will move inwards and the vortex will not only intensify, but contract. The increasing dominance of boundary layer friction is evident in Ex-4, Ex-5 and Ex-6, in which there is an increasingly strong signature of boundary-layer induced outflow above a height of about 500 m. This signature moves radially inwards and becomes deeper as the heating becomes weaker. As shown below, the radial flow at a height of 1 km at the location of the M-surface to which the heating is tied is positive in Ex-4, Ex-5 and Ex-6 and explains why these vortices weaken in intensity with time.

Figure 3 shows radius-height cross sections of the radial and tangential flow components at the initial time in Ex-1 and Ex-4, Ex-5 and Ex-6. In Ex-1 there is a deep layer of inflow throughout the lower troposphere (below about 5 km). In contrast, in Ex-4 and Ex-5, the inflow has weakened and in Ex-5 it has become confined to radii beyond the axis of the heating. Even in Ex-4 there is outflow on the axis of heating at a height of 1 km. In Ex-4, Ex-5 and Ex-6, there is a layer of low-level outflow that is induced by the boundary layer. In Ex-4, this layer starts first at a radius of nearly 175 km, but in Ex-5 and Ex-6 it extends all the way to the axis. In Ex-6, the heating is too weak to produce any inflow in the lower troposphere above the boundary layer. The behaviour of U_{max} and minimum U_{min} in panels (b) and (c) of Figure 1 at the initial time are in line with expectations emerging from Figure 3. Suffice it to say that in Ex-2 and Ex-3, the secondary circulation is qualitatively similar to that for Ex-1 in Figure 3(a) and of course the maximum inflow and outflow are stronger on account of the stronger heating rate.

2.3. *Flow structure at 18 h*

Figure 4 shows radius-height cross sections of the radial and tangential flow components at 18 h in Ex-1 and Ex-4 to Ex-6, which is beyond the time for which regularization is required in all these experiment. These should be compared with the corresponding fields in Figure 3. In Ex-1, the M-surfaces have moved inwards in the lower troposphere, except near the surface where the inward movement is opposed by the frictional torque. Thus, the M-surfaces develop a nose-like structure in the lower troposphere. As a result, V_{max} is located at a height of about 4 km at this time.

In the heated region, which has moved inwards by about 5 km since the initial time, the M-surfaces have moved upwards, but beyond this region, throughout much of the

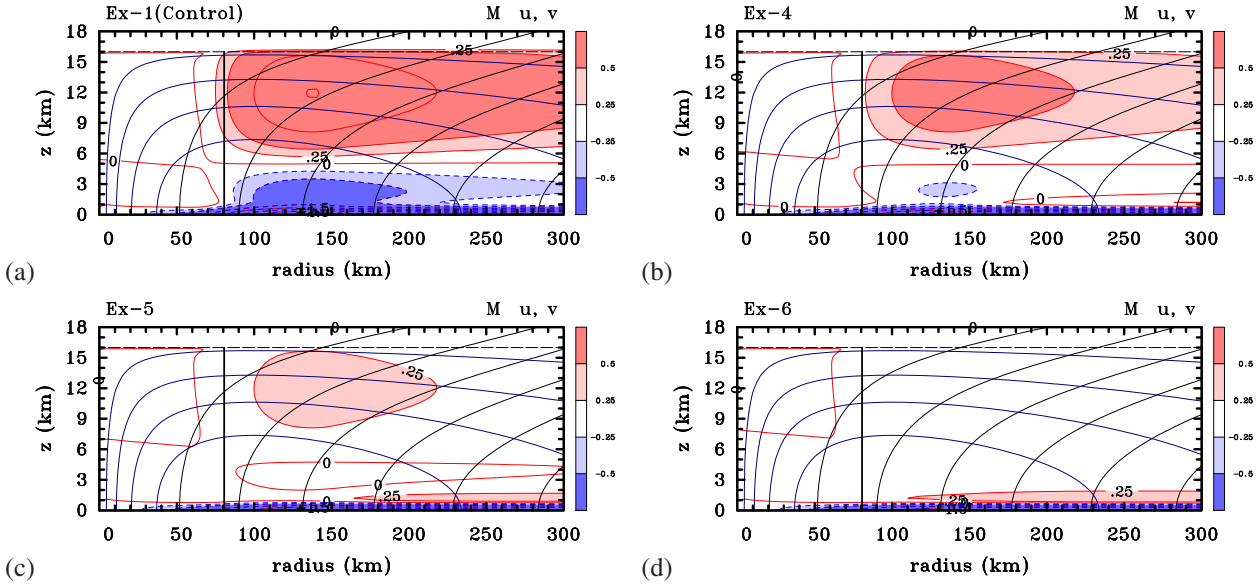

Figure 3. Radius-height cross sections of M-surfaces superimposed on the contours of tangential velocity, v, (solid blue contours) and radial velocity u (shaded) at the initial time. Contour interval for M, 5 $\times 10^5$ m^2 s^{-1}; for u, 0.5 m s^{-1} (shown also is the $u = 0.25$ m s^{-1} contour); for v, 2 m s^{-1}. Positive values (solid), negative values (dashed).

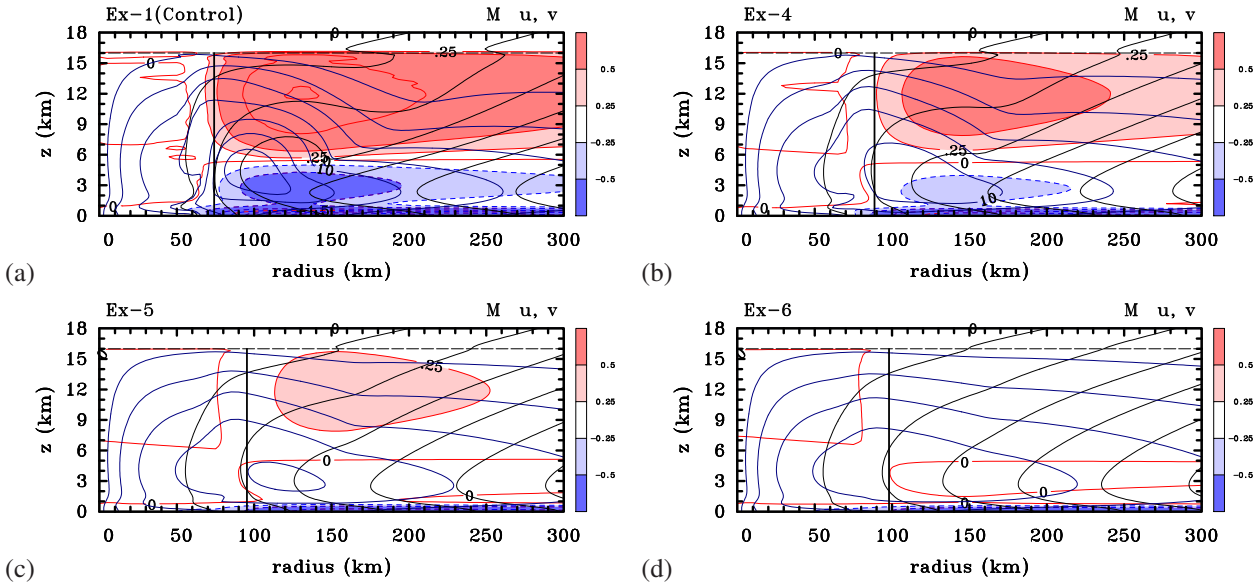

Figure 4. Radius-height cross sections of M-surfaces superimposed on the contours of tangential velocity, v (solid blue contours), and radial velocity u (shaded) at 18 h. Contour interval for M, 5 $\times 10^5$ m^2 s^{-1}; for u, 0.5 m s^{-1} (shown also is the $u = 0.25$ m s^{-1} contour); for v, 2 m s^{-1}. Positive values (solid), negative values (dashed).

troposphere they have descended. As shown in SMB, the descent is associated with subsidence beyond the region of heating. This subsidence is particularly strong just outside the region of heating to the extent that it leads to a negative radial gradient of M and thereby to a region of inertial instability (see subsection 2.4). The foregoing behaviour is similar in Ex-2 and Ex-3 (not shown).

In Ex-4, Ex-5 and Ex-6, the radial flow at a height of 1 km is slightly positive at the axis of heating, whereupon the heating axis moves slowly outwards with time. At 18 h the axis is located near 90 km radius in Ex-4, 95 km in Ex-5 and nearly 100 km in Ex-6. As in Ex-1, the M surfaces at 18 h all exhibit the inward-pointing nose like structure in the lower troposphere on account of the frictional torque and there is some elevation of these surfaces in the region of heating, but of course, this elevation is less pronounced when the heating is weaker. Moreover, weaker heating is accompanied by weaker subsidence outside the region of heating and only in Ex-4 is the subsidence strong enough to produce a negative radial gradient of M.

2.4. *Potential vorticity structure at 18 h*

Figure 5 shows radius-height cross sections of the potential vorticity (PV) distribution at 18 h in Ex-1 and Ex-4 to Ex-6. A prominent feature is the development of a region beyond the heating region in Ex-1 and Ex-4 where the PV is negative, a region in which the flow is symmetrically unstable. In Ex-5 and Ex-4 the PV field shows merely a tower of reduced values in this location.

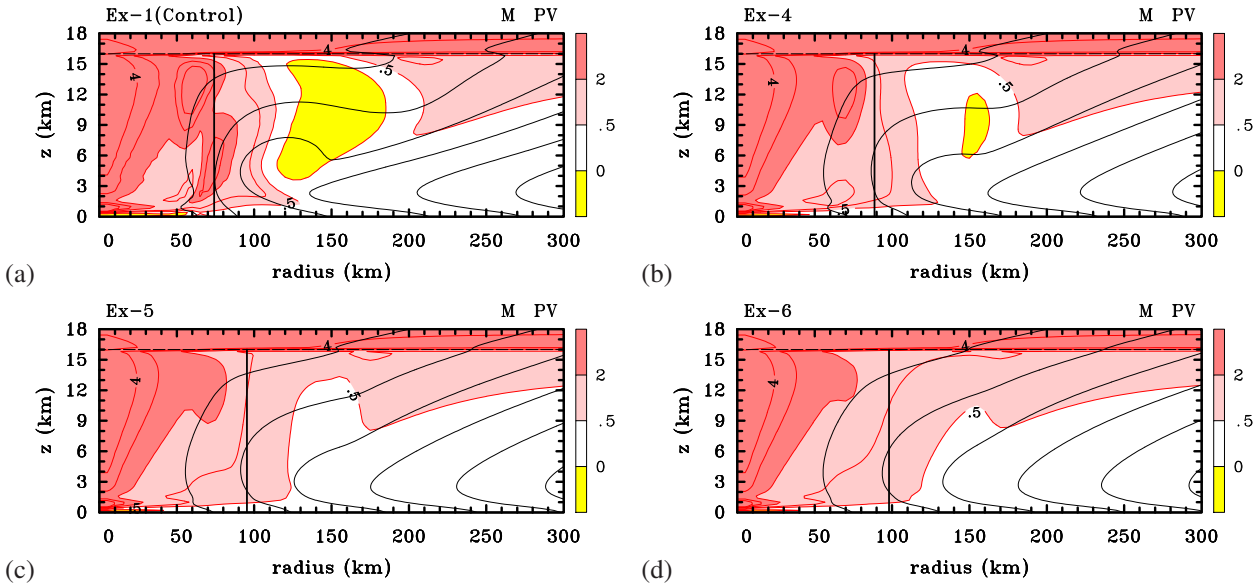

Figure 5. Radial-height cross sections of M-surfaces superimposed on the potential vorticity, PV (shaded) at 18 h. Contour intervals are: for M 5 $\times 10^5$ m^2 s^{-1}; for PV, 1 PV unit (= 1×10^{-6} m^2 s^{-1} K kg^{-1}). Shown also is the 0.5 PV unit contour.

2.5. *Pathological nature of the balanced boundary layer*

It is worth remarking on the somewhat pathological nature of the boundary layer that is highlighted by the foregoing solutions. It will be noticed in Figure 3 that, although at the initial instant, a fully developed layer of inflow is present on account of the specified boundary layer friction, no such boundary layer is evident in the tangential wind field at this time. In particular the M-surfaces intersect the surface at right angles, consistent with the prescribed zero vertical gradient of tangential velocity at the initial time. In essence, the tangential wind experiences the initially-imposed frictional torque through Equation (1) and it takes time for the near surface wind to be decelerated. In contrast, in the balance boundary layer formulation, the radial velocity component is determined by the need keep the tangential flow in balance, in part in the presence of the frictional torque and the inflow boundary layer is fully developed, even at the initial instant. Note that in this boundary layer formulation, there is no component of frictional force in the radial direction. Thus, while the balance formulation produces a vertical structure of inflow that is qualitatively similar to a true boundary layer, even at the initial instant, the same cannot be said for the tangential component, which, as our solutions show, takes a significant time (i.e. many hours) to develop. Moreover, in a true boundary layer, which a scale analysis shows not to be in gradient wind balance, the process that determines the inflow, at least at radii somewhat beyond the radius of maximum gradient wind is the frictional retardation of the tangential flow near the surface (see e.g. Smith and Vogl (2008) and refs.). This retardation makes the near-surface flow subgradient, leaving a net inward pressure gradient force to drive the inflow.

The foregoing considerations do not support the recent claim by Heng et al. (2017) that " ... balanced dynamics can well capture the secondary circulation in the full-physics model simulation *even in the inner-core region in the boundary layer* (italics are our emphasis)", a claim that has been refuted by Montgomery and Smith (2018).

3. Summary and conclusions

We have carried out a series of calculations with the axisymmetric prognostic balance model for tropical cyclone intensification developed recently by SMB. The calculations were designed to explore the interplay between the contributions to the secondary circulation from diabatic heating in eyewall convection and surface friction.

Radially outside the imposed heating region, diabatic heating, a proxy for deep cumulus convection, tends to produce a deep overturning circulation with inflow in the lower troposphere and outflow in the upper troposphere. In contrast, friction tends to produce a shallow overturning circulation with a layer of inflow near the surface and outflow in the lower troposphere above the boundary layer. Our calculations exemplify these competing tendencies in the lower troposphere, showing that vortex intensification requires the diabatic heating rate to be strong enough to ventilate the inflow in the frictional boundary layer, thereby averting frictionally-induced outflow just above the boundary layer.

A similar behaviour is found in numerical simulations with three-dimensional cloud-permitting simulations (see e.g. Kilroy et al. (2016) and refs.) and it is presumably a feature in the behaviour of real storms. In essence, sustained vortex intensification requires the diabatic heating rate to be strong enough to ventilate the inflow in the frictional boundary layer, thereby averting frictionally-induced outflow just above the boundary layer. Of course, in real storms, the strength and location of diabatic heating will be strongly influenced by the boundary layer dynamics and thermodynamics as discussed in Kilroy et al. (2016). This coupling is not present in the present balance model.

Notwithstanding the qualitative realism of the interplay between convective heating and frictional forcing exhibited by the balance solutions, the solutions do highlight the pathological nature of a "balanced boundary layer" as discussed in the text, a fact that, by itself cast a shadow on the conclusions of a recent paper claiming that balanced dynamics can well capture the secondary circulation in the

full-physics model simulation even in the inner-core region in the boundary layer.

Acknowledgements

We thank our colleagues Gerard Kilroy and Michael Montgomery for their perceptive comments on an earlier version of the manuscript. RKS acknowledges financial support for tropical cyclone research from the Office of Naval Research Global under Grant N62909-15-1-N021. SW acknowledges a Ph. D. stipend from the China Scholarship Council.

References

Bui, H. H., R. K. Smith, M. T. Montgomery, and J. Peng, 2009: Balanced and unbalanced aspects of tropical-cyclone intensification. *Quart. Journ. Roy. Meteor. Soc.*, **135**, 1715–1731.

Dunion, J. P., 2011: Rewriting the climatology of the tropical north atlantic and caribbean sea atmosphere. *J. Clim.*, **24**, 893–908.

Emanuel, K. A., 1997: Some aspects of hurricane inner-core dynamics and energetics. *J. Atmos. Sci.*, **54**, 1014–1026.

— 2012: Self-stratification of tropical cyclone outflow. Part II: Implications for storm intensification. *J. Atmos. Sci.*, **69**, 988–996.

Heng, J., Y. Wang, and W. Zhou, 2017: Revisiting the balanced and unbalanced aspects of tropical cyclone intensification. *J. Atmos. Sci.*, **74**, 2575–2591.

Kilroy, G., R. K. Smith, and M. T. Montgomery, 2016: Why do model tropical cyclones grow progressively in size and decay in intensity after reaching maturity? *J. Atmos. Sci.*, **73**, 487–503.

Montgomery, M. T. and R. K. Smith, 2018: Comments on: Revisiting the balanced and unbalanced aspects of tropical cyclone intensification, by J. Heng, Y. Wang and W. Zhou. *J. Atmos. Sci.*, **75**, xxx–xxx.

Ooyama, K. V., 1969: Numerical simulation of the life cycle of tropical cyclones. *J. Atmos. Sci.*, **26**, 3–40.

Smith, R. K., M. T. Montgomery, and H. Bui, 2018: Axisymmetric balance dynamics of tropical cyclone intensification and its breakdown revisited. *J. Atmos. Sci.*, **75**, xxx–xxx.

Smith, R. K. and S. Vogl, 2008: A simple model of the hurricane boundary layer revisited. *Quart. Journ. Roy. Meteor. Soc.*, **134**, 337–351.

Willoughby, H. E., 1979: Forced secondary circulations in hurricanes. *J. Geophys. Res.*, **84**, 3173–3183.